Research Article | Vol. 27, No. 22 / 28 October 2019 / Optics Express 31176
Optics EXPRESS

Superradiant diamond color center arrays coupled to concave plasmonic nanoresonators

DÁVID VASS,[1,3] ANDRÁS SZENES,[1,3] BALÁZS BÁNHELYI,[2] TIBOR CSENDES,[2] GÁBOR SZABÓ,[1] AND MÁRIA CSETE[1,*]

[1]Department of Optics and Quantum Electronics, University of Szeged, Dóm tér 9, Szeged 6720, Hungary
[2]Department of Computational Optimization, University of Szeged, Árpád tér 2, Szeged 6720, Hungary
[3]These authors equally contributed to this study
[*]mcsete@physx.u-szeged.hu

Abstract: Superradiantly enhanced emission of SiV diamond color centers was achieved via numerically optimized concave plasmonic nanoresonators. Advantages of different numbers of SiV color centers, diamond-silver (bare) and diamond-silver-diamond (coated) core-shell nanoresonator types, spherical and ellipsoidal geometries were compared. Indistinguishable superradiance is reached via four color centers, which is accompanied by line-width narrowing except in a coated ellipsoidal nanoresonator that outperforms its bare counterpart in superradiance. Seeding of both spherical and bare ellipsoidal nano-resonators with six color centers results in larger fluorescence enhancement and better overridden superradiance thresholds simultaneously. Both phenomena are the best optimized in a six color centers seeded ellipsoidal bare nanoresonator according to the pronounced bad-cavity characteristics.

1. Introduction

The superradiance (SR) predicted first by Dicke has been thoroughly studied throughout the last half-century [1,2]. In case of cooperativity N emitters can exhibit N-times shorter radiative decay, accordingly the maximum rate of emission can be proportional to N^2. Contradicting predictions also appeared in the primary literature about that the coherence can be lost caused by spatially varying frequency shift [3]. However, the statements about that Dicke effect can be achieved either via systems, which are initially in "collective Dicke" state, or via transient amplification of the photon noise, are widely accepted by the scientific community [4,5]. In sub-wavelength emitter arrays the non-uniform distribution of initial phases is the pre-condition of a superradiant burst development [6]. The SR phenomenon has been already widely inspected in systems, which are either significantly smaller or larger than the wavelength [7,8]. A particularly important fundamental phenomenon is the Dicke quantum phase transition inside an optical cavity [9–11].

An emerging research area is investigation of the plasmonic Dicke effect (PDE). The simplest systems that exhibit plasmon mediated superradiance are coupled waveguides, and preference to channels and existence of optimal configurations had been revealed in the earliest studies [12]. Later spherical plasmonic nanoresonators (NR) were inspected, and PDE was achieved via arrays of emitters around a solid plasmonic particle [13–15]. In these studies the phase of dipolar emitters was supposed to be random, whereas their orientation was uniformly perpendicular to the solid plasmonic nanoparticle interface. Random spatial distribution [13] and a fullerene-like spherical lattice [14,15] were considered as well. Both the direct coupling through radiation and the indirect coupling through plasmons were taken into account. The main conclusions were that the plasmon assisted coupling overrides the direct radiative coupling between emitters, the total radiative rate enhancement is proportional to $N/3$, whereas the total energy is thrice of the individual emitter energy.

The plasmon mediated cooperative coupling phenomena were analyzed in similar systems consisting of a spherical metal core covered by a gain medium shell, by taking into account

#368660 https://doi.org/10.1364/OE.27.031176
Journal © 2019 Received 31 May 2019; revised 8 Aug 2019; accepted 10 Sep 2019; published 14 Oct 2019

Optics EXPRESS

all mutual couplings and by treating the dye via an equivalent polarizability [16]. The effect of a metallic nanoparticle embedded into a symmetric array of already collectively oscillating dipolar emitters was inspected as well [17]. However, to achieve a collective Dicke state the indistinguishable nature of emitters manifesting itself in synchronized phases was required. In these studies all dipolar emitters were aligned parallel and equidistantly, which ensured that only symmetric states could be at play and only one single plasmon could be excited. It was demonstrated that the nanoparticle accelerates the superradiance, decreases the SR pulse delay as well as its duration. The robustness of cooperativity related insensitivity to spatial and polarization disorder was demonstrated, and it was shown that emitter-emitter interactions alter the cooperativity only at their large densities [18].

The Purcell-Dicke effect of an atomic ensemble near a conducting surface was qualified by the Purcell fidelity that exhibits a superradiant burst in its dynamics [19]. It was demonstrated that the metal surface mediated collective interactions can lead to superradiance (subradiance) in case of constructive (destructive) interference between emitters [20]. Switching into a plasmon-mediated superradiant state via cooling was attributed to polarization phase matching of the molecular transitions in emitters embedded into a dielectric shell around a gold core [21]. It is important to notice that in all previous examples of plasmonic superradiance - except the few cases in [12–15,18] - all emitters are in an excited, moreover in a synchronized collective Dicke state [15–16,19–21].

The Purcell-Dicke effect was demonstrated in concave nanoresonators as well, namely in an ensemble of resonant atoms, which are embedded into a spherical dielectric core coated by a metallic shell [22,23]. Existence of one and two superradiant modes was proven by neglecting [22] and taking into account [23] the wavelength dependency of the optical parameters. Superradiant source's tuning was demonstrated by tailoring the interaction of localized and lattice plasmon resonances via arrays of ring-shaped nanoresonators fed by coherent emitters [24]. An array of cylindrical concave NRs embedded into a metal film was also applied to generate SR, and it was shown that a cw superradiance is achievable due to the synchronization of plasmonic nanoholes via gain molecules [25]. Intense coherent light can be extracted into the far-field via directed beams out-coupled by such a 2D spaser array.

Among important applications of the photonic superradiance is design of superradiant lasers, which exhibit ultra-narrow lines [26]. It has been demonstrated that the quantum measurement precision can be improved via squeezed Dicke states [27]. Dicke superradiance in two qubits ensembles makes it possible to explore different aspects of entanglement [28]. There are emerging applications of the plasmonic superradiance as well. An ordered radial arrangement of few dipolar emitters around a solid plasmonic sphere was inspected as a potential candidate for a multi-qubits deterministic quantum phase gate [29]. In this approach the emitter-emitter interactions have been ignored, whereas the plasmon mediated long-range interactions have been taken into account. In Ag doped oxyfluoride, for which the wide nanoparticle band and the size-dependent cluster band overlap mediates the Ag nanoclusters interaction, the plasmonic Dicke effect can be used to generate picosecond pulses [30].

Diamond is a promising candidate, since superradiance was already demonstrated from NV centers in diamond nanocrystals [31]. It was shown that the bright diamond nanocrystals are faster, and a decay rate enhancement in the order of 0.9xN-fold was reported. The second order correlation function proved the cooperative nature of diamond nanocrystal's emission in certain configurations. Moreover, cooperatively enhanced trapping was also demonstrated in nanodiamonds consisting of large density NV centers [32]. SiV is a particularly promising diamond color center due to the achievable stronger transition moment and the resulted narrow fluorescence line [33–36]. Both in bulk and in nanofabricated diamond the almost lifetime limited line-width of SiV is accompanied by an extremely small inhomogeneous broadening, which is the precondition to generate indistinguishable photons [35,36]. Although, it has

Optics EXPRESS

been already predicted that the most efficient radiation escaping can be ensured via optimized concave core-shell nanoparticles [22], the previously investigated plasmonic nanoresonators did not possess the optimal configurations [12–25,29,30]. Plasmon enhanced fluorescence of different diamond color centers has been already demonstrated via individual and arrayed concave plasmonic nanoresonators [37–41]. Considerable lifetime reduction was observed via coupled nanodiamonds and metal nanowires as well as via nano-assembled metal-diamond hybrid structures [42,43]. Superradiant emission of silicon vacancy centers (SiV) in a diamond zero index metamaterial has been recently reported [44]. However, plasmonically boosted superradiance in diamond has not been demonstrated previously.

In our present study we demonstrate that symmetrical arrays of diamond color centers in optimized concave plasmonic nanoresonators make it possible to achieve not only fluorescence enhancement but also superradiantly enhanced emission.

2. Methods

Concave spherical and ellipsoidal core-shell nanoresonators have been optimized to maximize the fluorescence rate from various arrays of multiple SiV color centers treated as dipolar emitters by using a FEM (COMSOL Multiphysics) based method described in our previous publications (Figs. 1–6, see Visualization 1, Visualization 2, Visualization 3, Visualization 4, Visualization 5, Visualization 6, and Visualization 7) [37–39,45,46]. Growth of such spherical nanodiamonds would be possible in plasma, where the diamond core nucleus could levitate as a result the substrate effect could be eliminated, whereas post-coating by metal layers is possible via chemical procedures [47]. The inspected ellipsoidal nanoresonators are similar to metal coated nanowires that can be fabricated via e-beam lithography [40,41]. The amount of SiV color centers can be significantly large in nanodiamonds, in this study 4 and 6 numbers of color centers were selected, since their arrays can be selectively excited in nanoresonator lattices of four- and six-fold symmetry via in-coupled far-field illumination.

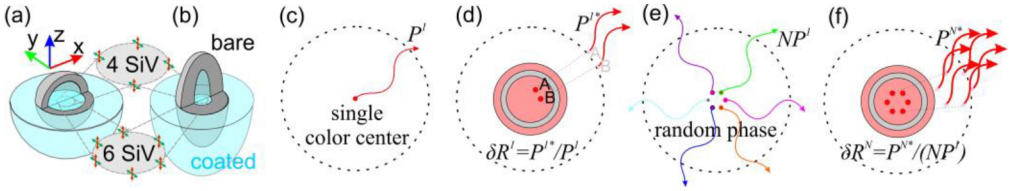

Fig. 1. Schematics of the optimized coupled system types: (a) spherical and (b) ellipsoidal nanoresonators, that can be seeded with 4 and 6 emitters as well as bare and coated type. (c-f) Schematics of vacuum reference systems consisting of (c) one single emitter and (e) N emitters with random phases to calculate radiative rate enhancements. Concave plasmonic core-shell nanoresonator enhanced coupled systems to determine: (d) single emitter enhancement in the reference coupled system for superradiance evaluation and (f) N collectively oscillating emitter's enhancement, which qualifies the superradiantly enhanced optimized coupled system. P^1 and NP^1: power radiated by one single emitter and N randomly oscillating emitters in vacuum, P^{1*} and P^{N*}: enhanced power radiated by one single emitter and N collectively oscillating emitters inside the optimized nanoresonator, δR^1 and δR^N: radiative rate enhancement achieved via one single emitter and via N collectively oscillating emitters. More details are provided in Visualization 1 and Visualization 2.

The inspected spherical (ellipsoidal) NRs consist of a symmetrical square and hexagonal array of 4 and 6 SiV color centers, which oscillate in the equatorial plane (corresponding to the short axis) at the excitation and perpendicular to it (along the long axis) at the emission, according to the SiV color center transition dipole's perpendicularity. Diamond-silver core-shells standing in air are referred to as bare type NRs, whereas core-shells of the same composition covered by an

Optics EXPRESS

additional diamond layer are referred to as coated type NRs (Figs. 1(a) and 1(b), Fig. 3 insets, see Visualization 1). The wavelength dependent complex dielectric function of silver was loaded by interpolating measured datasets from the literature with spline-fits, whereas the wavelength dependent refractive index of diamond was defined by its Cauchy formula, as in our previous works [37–39,46,48].

In our previous studies we have determined the radiative rate enhancement in plasmonic environments [37–39]. By supposing that the emitter does not have an intrinsic loss and no quenching occurs at the specific emitter-metal distance, the *Purcell factor* can be computed as the ratio of powers radiated by the emitter into the far-field and absorbed by the NR to the power radiated by the emitter in a homogeneous medium:

$$Purcell\ factor = (P_{\text{radiative}} + P_{\text{non - radiative}}) \big/ P_{\text{radiative\_0}}. \tag{1}$$

Under the same circumstances the quantum efficiency can be computed as:

$$QE = P_{\text{radiative}} / (P_{\text{radiative}} + P_{\text{non - radiative}}), \tag{2}$$

accordingly, the radiative rate enhancement is:

$$\delta R = Purcell\ factor \times QE = P_{\text{radiative}} \big/ P_{\text{radiative\_0}}, \tag{3}$$

whereas the achieved QE can be corrected by taking into account the non-unity QE_0 of SiV:

$$cQE = \delta R / (Purcell\ factor + (1 - QE_0) / QE_0). \tag{4}$$

The optimization was performed by selecting $P_{\text{x}}cQE$ as the objective function, which is the product of radiative rate enhancements at the excitation (δR_{ex}) and emission (δR_{em}), nominated as P_{x} *factor*, and the quantum efficiency at the emission (cQE), which is corrected by the 10% intrinsic quantum efficiency of SiV color centers [37–39,46]. Conditional optimizations were performed via an in-house developed algorithm integrated into COMSOL software package [45]. According to the radiative rate criterion set at the excitation, only those systems were evaluated, which ensured excitation enhancement as well. The optimized NRs were characterized by their scattering (*scs*) and extinction (*ecs*) cross-sections determined via linearly polarized plane wave illumination (Fig. 2(a), see Visualization 6). Ellipsoidal NRs were illuminated by a plane wave with a polarization along their short and long axis to determine the optical cross-sections in the excitation and emission configurations. To qualify bare and coated type spherical and ellipsoidal NRs seeded with 4 and 6 SiV color centers, the wavelength dependent quantum efficiency (QE), *Purcell factor* and radiative rate enhancement (δR) have been determined (Figs. 2(a)–2(c), see Visualization 3).

The optimized NRs are capable of resulting in δR^1 radiative rate enhancement of one single SiV color center (Figs. 1(c) and 1(d)). The δR^{N} radiative rate of N SiV color centers collectively oscillating inside NRs was determined by comparing their $P^{\text{N}*}$ radiated power to the N-fold of the P^1 power radiated by one single SiV color center oscillating in vacuum, i.e. existence of initially randomly oscillating color centers was supposed (Figs. 1(e) and 1(f)). Selection of randomly oscillating SiV color centers in vacuum as a reference system ensures that the optimized NRs result in superradiantly enhanced emission, rather than a plasmonically enhanced superradiance, which has been previously described in the literature [17]. The surface charge density and near-field distributions as well as the far-field radiation pattern were inspected at the SiV color center 532 nm excitation and 737 nm emission wavelengths (Fig. 3 and Fig. 4, see Visualization 3). To quantify and compare different optimized systems the P_{x} *factor* and $P_{\text{x}}cQE$ were determined for different numbers of color centers, different NR types and geometries (Fig. 5(a), see Visualization 3(d)).

Optics EXPRESS

From both the vacuum reference and nanoresonator coupled systems seeded with one single and N SiV color centers the radiated power was read out. However, rearrangement of Eq. (5a) results in Eq. (5b) and comparison of Eq. (5b) and Eq. (6a) shows that consideration of "radiative rate enhancement ratio larger than N emitter number" criterion both at the excitation and emission in Eq. (6a) is equivalent with the conventional criterion of a superradiance achievement regarding the emitted power in Eq. (6b) (Figs. 1(c)–1(f)).

$$\mathrm{r}\delta R = \delta R^{\mathrm{N}} \Big/ \delta R^{1} = (P^{\mathrm{N}*} \Big/ NP^{1}) \Big/ (P^{1*} \Big/ P^{1}) = P^{\mathrm{N}*} \Big/ (NP^{1*}), \tag{5a}$$

$$N\mathrm{r}\delta R = P^{\mathrm{N}*} \Big/ P^{1*}, \tag{5b}$$

$$N < \mathrm{r}\delta R, \tag{6a}$$

$$N^{2} < P^{\mathrm{N}*} \Big/ P^{1*}. \tag{6b}$$

Accordingly, to prove that superradiance is achievable via N color centers in the optimized configurations, the δR^{N} radiative rate enhancements both at the excitation and emission were compared to corresponding δR^{1} of the reference systems consisting of one single SiV color center inside a NR having the specific geometry (Fig. 1 and Fig. 5(b), see Visualization 4(a)).

The optical responses of reference systems were calculated by taking the average of responses in all distinguishable, i.e. geometrically different, SiV color center positions (Fig. 1(d)). Namely, the optical response in one single color center position was determined in both configurations of $N = 4$ centers and in the emission configuration of $N = 6$ centers in both types of spherical and ellipsoidal NRs. In contrast, the optical responses in the two distinguishable, i.e. geometrically different single color center positions were averaged in the excitation configuration of all NRs seeded with $N = 6$ color centers. For the sake of completeness, the cQE corrected quantum efficiency achievable via N color centers and via one single center were compared, finally the ratio of the P_{x} *factors* and the ratio of the $P_{\mathrm{x}}cQE$ objective function values was also determined (Fig. 5(b), see Visualization 4).

To conclude about the superradiance the ratios with respect to the reference system were normalized as follows: $\mathrm{r}\delta R_{\mathrm{ex}}/N$, $\mathrm{r}\delta R_{\mathrm{em}}/N$, $\mathrm{r}P_{\mathrm{x}}/N^{2}$, $\mathrm{r}P_{\mathrm{x}}cQE/N^{2}$and $\mathrm{r}cQE/1$, where $\mathrm{r}X$ refers to the ratio of specific quantities, N indicates the number of embedded color centers. That means we consider N and N^{2} as the balanced partial and complete multiplied thresholds of superradiance, respectively. However, these thresholds are equivalent with the usual criterion of superradiance required for the radiated power, which has to be proportional to N^{2}, as it is described in Eqs. (5)–(6) (Fig. 1, see Visualization 5). Finally, the average of the normalized ratios ($\overline{rX}=\Sigma(\mathrm{r}\delta R_{\mathrm{ex}}/N, \mathrm{r}\delta R_{\mathrm{em}}/N, \mathrm{r}P_{\mathrm{x}}/N^{2}, \mathrm{r}(P_{\mathrm{x}}cQE)/N^{2}, \mathrm{r}cQE/1)/5$) was determined, to evaluate the superradiance overriding on the average (Fig. 5(b), see Visualization 5(d)).

In order to qualify the linearly polarized plane-wave illuminated and N color center seeded optimized NRs, the FWHM of extinction and scattering cross-section peaks was determined and compared to the FWHM of *Purcell factor* and δR radiative rate enhancement peaks (Fig. 5(c), see Visualization 6(a)). The quality factor (*Q factor*) of the optimized NRs was determined based on the extinction cross-section and *Purcell factor* spectral peaks (Fig. 5(c), see Visualization 6(b)). To qualify the cooperatively oscillating emitters, detuning ($\Delta\lambda$) of the extinction and scattering cross-section peaks, *Purcell factor* and δR radiative rate enhancement peaks from the SiV color center emission wavelength as well as the frequency pulling ($\Delta f = f_{ecs}\text{-}f_{\delta R}$) were determined (Fig. 5(d), see Visualization 6 [26].

To analyze, if all N color centers are indistinguishable, degeneracy in *Purcell factor* was inspected at the excitation and emission wavelengths as well (Figs. 6(a) and 6(b), see Visualization 7). Comparison of P_{x} *factor* and $P_{\mathrm{x}}cQE$ achievable via systems consisting of collectively and randomly oscillating color centers inside the optimized NRs was also performed (Figs. 6(c) and

Optics EXPRESS

6(d)). All comparative statements are presented in 4-to-6 SiV color centers, bare-to-coated NR type, ellipsoidal-to-spherical NR geometry sequence. In case of emission comparative statements with respect to the excitation are also presented. All quantities presented in the paper qualify coupled systems consisting of N SiV color centers.

The results in the paper prove the achievement of superradiance in the optimized concave nanoresonators and are self-consistent themselves, whereas further information is provided in Visualization 1, Visualization 2, Visualization 3, Visualization 4, Visualization 5, Visualization 6, and Visualization 7 to ensure detailed comparison with reproduceable results.

3. Results and discussion

The appropriately large distances between SiV color centers in the optimized NRs allow neglecting their direct coupling, similarly to previous studies in the literature [18,29]. The optimal distances of SiV centers from the metal is inside the interval, where color center's mean depth can be defined via ion implantation of a suitable energy based on SRIM simulations [49,50]. All geometrical parameters, including R core radii, t shell thickness, d SiV color center distance from the metal shell are very similar, when 4 and 6 SiV color centers are embedded into the same bare or coated types of optimized NRs (Figs. 1(a) and 1(b), see Visualization 1 and Visualization 2). The similar characteristics in case of 4 and 6 centers reveal that by increasing the number of embedded emitters the geometrical parameters of the optimized NRs only slightly modify, as it has been proven by complementary studies.

The absence of additional shell has a well-defined effect on the optimal geometrical parameters, namely the core radius is larger and the shell thickness is smaller. Accordingly, the generalized aspect ratio ($GAR = R/(R + t)$ ratio of inner and outer radii) is larger, and the SiV center distance is larger in optimized bare spherical nanoresonators compared to their coated counterparts. Similarly, the larger long axis and the smaller shell thickness results in larger GAR, whereas the SiV center distance is larger (the same) in 4 (6) color center seeded bare ellipsoidal nanoresonators, compared to their coated counterparts. The long axis of ellipsoidal NRs is commensurate with the radius of spherical NRs of the same type, whereas the shell thickness is ~1.6 (2.2)-times larger, accordingly the GAR corresponding to the long axis is commensurate with the GAR in spherical NRs. The SiV color center's distance is the ~fourth (half) in bare (coated) ellipsoidal NRs, compared to those in their spherical counterpart.

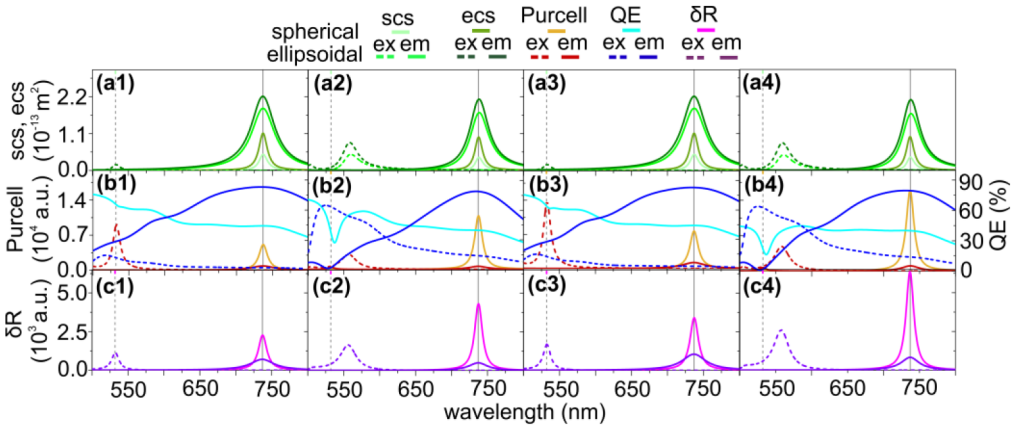

Fig. 2. The (a) scattering (*scs*) and extinction (*ecs*) cross-section, (b) *Purcell factor* and *QE* quantum efficiency, (c) δR radiative rate enhancement spectra of (a1, b1, c1) bare_4, (a2, b2, c2) coated_4, (a3, b3, c3) bare_6 and (a4, b4, c4) coated_6 spherical and ellipsoidal NRs. More details are provided in Visualization 3 and Visualization 6.

Optics EXPRESS

The general characteristic of the optical signals is very similar in NRs with a specific geometry (Fig. 2). In all optimized spherical NRs a single peak appears on the extinction and scattering cross-section, as well as on the *Purcell factor* and δR radiative rate enhancement spectrum at the emission wavelength (Figs. 2(a)–2(c)). In contrast, in the excitation / emission configuration of the optimized bare (coated) ellipsoidal NRs the global maximum appears at (close to) the 532 nm excitation / 737 nm emission wavelength on all spectra. In addition to this a local maximum develops on the extinction cross-section at the excitation wavelength in the emission configuration of coated ellipsoidal NRs (Figs. 2(a2) and 2(a4)).

On the quantum efficiency spectrum of all optimized spherical NRs there is a minimum at the excitation, whereas a local maximum appears at the emission (Fig. 2(b)). The minimum at the excitation is a global minimum in coated spherical NRs.

In contrast, a global maximum appears on the *QE* spectrum close to the excitation and at the emission wavelength in corresponding configurations of ellipsoidal NRs. The global maximum is significantly larger in the emission than in the excitation configuration of bare ellipsoidal NRs, whereas it is just moderately larger in coated ellipsoidal NRs (Fig. 2(b)).

The time-dependent surface charge density distribution at the excitation is noticeably hexagonal on bare spherical and ellipsoidal NRs, whereas on coated NRs a dominantly hexagonal distribution develops, which is more characteristic on coated spherical NRs (Figs. 3(a) and 3(b)). The charge distribution is permanently dipolar at the emission on all optimized spherical and ellipsoidal NRs (Figs. 3(c) and 3(d)). According to the orientation of dipolar emitters in corresponding configurations, the characteristic hexagonal charge distribution is antisymmetric along y (short) axis at the excitation, whereas the dipolar charge distribution is aligned along the z (long) axis on the spherical (ellipsoidal) NRs at the emission.

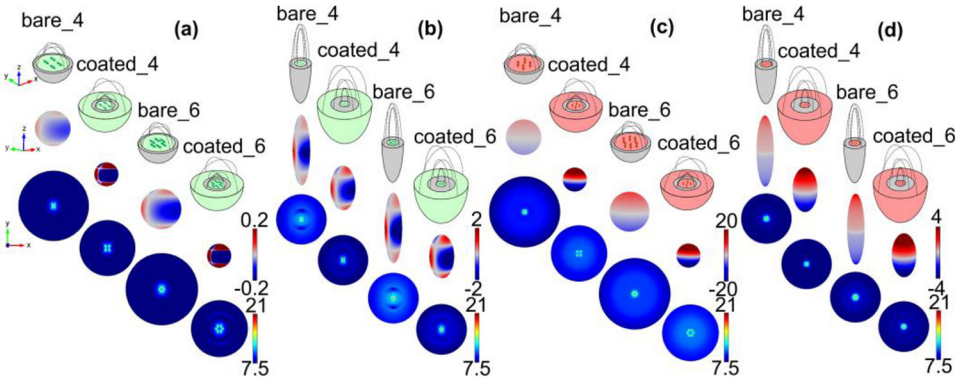

Fig. 3. Schematic drawings, characteristic surface charge density distribution and normalized **E**-field distribution of (a, c) spherical and (b, d) ellipsoidal NRs at the (a, b) excitation and (c, d) emission wavelength. More details are provided in Visualization 3.

3.1. Comparative study at the excitation

The achieved *QE* is always smaller in NRs consisting of 6 color centers, except in bare ellipsoidal NRs (Fig. 2(b), see Visualization 3(a)). In bare spherical NRs the larger core, smaller shell thickness and larger color center distance results in significantly larger *QE*. In contrast, in bare ellipsoidal NRs despite their larger long axis, thinner shell and larger (same) emitter distance in case of 4 (6) color centers, the *QE* is significantly smaller, than in their coated counterparts. Accordingly, the *QE* is significantly smaller in bare, whereas it is considerably larger in coated ellipsoidal NRs, than in their spherical counterparts.

Optics EXPRESS

The *Purcell factor* is in the order of 10 and 10^2 in the optimized bare and coated spherical NRs, whereas 10^4 and 10^3 *Purcell factors* are achieved via bare and coated ellipsoidal NRs, respectively (Fig. 2(b), see Visualization 3(b)). The *Purcell factor* is always larger in NRs consisting of 6 color centers due to the stronger charge accumulation. In bare spherical NRs consisting of 4 (6) SiV color centers the significantly larger emitter distance results in weaker charge accumulation and allows reaching 3 (4)-times smaller *Purcell factor*, than in their coated counterparts. In contrast, in bare ellipsoidal NRs independently of the number of embedded SiV color centers, the commensurate and same emitter distance makes it possible to achieve stronger charge accumulation and an order of magnitude larger *Purcell factor*, than in their coated counterparts. Accordingly, in bare and coated ellipsoidal NRs two and one orders of magnitude larger charge accumulation manifests itself in significantly and considerably larger *Purcell factor*, than in their spherical counterparts, respectively (Fig. 2(b), Figs. 3(a) and 3(b), see Visualization 3).

As a result, 4 and 6 (8 and 11)-fold excitation rate enhancement can be achieved in presence of 4 and 6 color centers in bare (coated) spherical NRs. In comparison, 10^3 (10^2)-fold excitation enhancement is achieved in bare (coated) ellipsoidal NRs consisting of either 4 or 6 color centers (Fig. 2(c), see Visualization 3(c)). Accordingly, the excitation rate enhancement is always larger in NRs consisting of 6 color centers, which manifests itself in larger far-field lobes (Figs. 4(a) and 4(b), see Visualization 3). In bare spherical NRs the smaller *Purcell factor* allows smaller excitation rate enhancement and far-field lobes despite the larger quantum efficiency, than in coated spherical NRs (Fig. 4(a), see Visualization 3). In contrast, in bare ellipsoidal NRs the one order of magnitude larger *Purcell factor* allows larger excitation rate enhancement and far-field lobes despite the significantly smaller quantum efficiency compared to their coated counterparts (Fig. 4(b), see Visualization 3). The achieved excitation rate enhancement is significantly and considerably larger in bare and coated ellipsoidal NRs, than in their spherical counterparts, which manifest themselves in larger lobes corresponding to the far-field radiated power (Figs. 4(a) and 4(b), see Visualization 3).

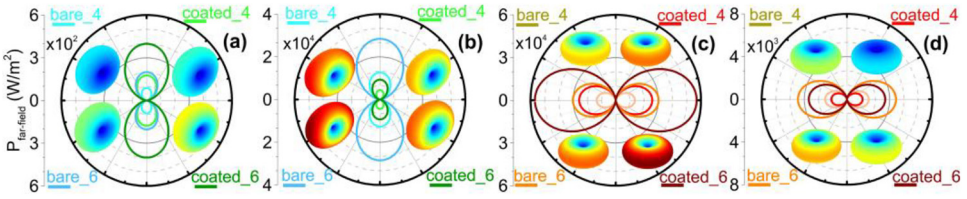

Fig. 4. Angular distribution of the far-field emitted power: (a, c) spherical and (b, d) ellipsoidal NRs at the (a, b) excitation and (c, d) emission wavelength. Insets: distribution of the power emitted into the far-field in 3D. The lobes on the angular distribution of the far-field radiated power are perpendicular to the y (z) axes at the excitation (emission) wavelength, revealing that the SiV color centers are efficiently coupled to each types of optimized concave plasmonic NRs. More details are provided in Visualization 3.

3.2. Comparative study at the emission

There is no significant difference between the corrected quantum efficiencies achieved in case of seeding with 4 and 6 color centers in neither of spherical nor in ellipsoidal NRs (Fig. 2(b), see Visualization 3(a)). In bare type spherical and ellipsoidal NRs the larger core (long axis), smaller shell thickness and larger (same) emitter distance make it possible that the *cQE* at the emission is larger, than in their coated counterparts. Accordingly, the *cQE* is considerably larger both in bare and coated ellipsoidal NRs, than in their spherical counterparts.

Optics EXPRESS

Compared to the excitation, the *cQE* at the emission is considerably smaller in bare spherical NRs, more commensurate in coated_4 spherical NR, however it is larger in coated_6 spherical NR. In contrast, the *cQE* at the emission is larger in all ellipsoidal NRs than at the excitation, and the enhancement is significantly larger in bare ellipsoidal NRs.

The *Purcell factor* is in the order of 10^4 in spherical NRs, whereas 10^3 *Purcell factor* is achieved in ellipsoidal NRs, independently of diamond coating existence (Fig. 2(b), see Visualization 3(b)). In NRs consisting of 6 color centers both the accumulated charge and the *Purcell factor* are always larger at the emission as well. In bare spherical (4 and 6 color centers seeded bare ellipsoidal) NRs the significantly larger (commensurate and same) emitter distance results in weaker charge accumulation, than in their coated counterparts. In bare spherical NRs the smaller amount of charge allows to reach considerably smaller *Purcell factor*, whereas in bare ellipsoidal NRs makes it possible to achieve slightly larger *Purcell factor*, than in their coated counterparts. In bare and coated ellipsoidal NRs the amount of accumulated charge is slightly and one order of magnitude smaller, which manifests itself in considerably and significantly smaller *Purcell factor*, than in their spherical counterparts, respectively (Fig. 2(b), Figs. 3(c) and 3(d), see Visualization 3).

At the emission two orders of magnitude larger accumulated charge on the spherical NRs allows to reach typically three-orders of magnitude larger *Purcell factor* than those at the excitation, which reveals that stronger plasmonic resonance occurs at this wavelength. In contrast, at the emission the charge accumulation is slightly weaker in bare ellipsoidal NRs, whereas it is slightly stronger in coated ellipsoidal NRs, than those at the excitation. Accordingly, the *Purcell factor* at the emission is with one order of magnitude smaller in bare ellipsoidal NRs, whereas it is slightly smaller and larger in coated_4 and coated_6 ellipsoidal NRs, than that at the excitation. This reveals that the strength of resonance is more commensurate at the two wavelengths on ellipsoidal NRs.

As a result, 2×10^3 and 4×10^3 (4×10^3 and 7×10^3) emission rate enhancement can be achieved in presence of 4 and 6 color centers in bare (coated) spherical NRs. In comparison, 7×10^2 and 1×10^3 (5×10^2 and 8×10^2) emission rate enhancement can be achieved in presence of 4 and 6 color centers in bare (coated) ellipsoidal NRs (Fig. 2(c), see Visualization 3(c)). In NRs consisting of 6 color centers the radiative rate enhancement and far-field radiated power are always larger at the emission as well (Figs. 4(c) and 4(d), see Visualization 3). In bare spherical NRs despite the larger quantum efficiency, two-times smaller *Purcell factor* allows smaller emission rate enhancement and far-field lobes, than in their coated counterparts, similarly to the excitation (Fig. 4(c), Visualization 3). In contrast, in bare ellipsoidal NRs the larger *cQE* and *Purcell factor* makes it possible to reach larger emission rate enhancement and far-field lobes, than that achievable via coated ellipsoidal NRs (Fig. 4(d), Visualization 3). As a consequence, in bare and coated ellipsoidal NRs the emission rate enhancement and the far-field lobes are considerably and significantly smaller, than in their spherical counterparts, in contrast to the excitation (Figs. 4(c) and 4(d), Visualization 3).

The radiative rate enhancement in spherical NRs is typically three orders of magnitude larger at the emission than that at the excitation, which manifests itself in larger far-field lobes (Figs. 4(a) and 4(c), Visualization 3). In contrast, the radiative rate enhancement at the emission is smaller in bare ellipsoidal NRs, whereas in coated ellipsoidal NRs it is larger than at the excitation. However, the maximal extension of the far-field lobe is smaller at the emission revealing that the directivity is similarly smaller than at the excitation in both types of ellipsoidal NRs (Figs. 4(b) and 4(d), Visualization 3).

3.3. Total fluorescence enhancements

Considerably large 1×10^4 and 2×10^4 (4×10^4 and 8×10^4) complete fluorescence enhancement qualified by the P_x *factor* can be achieved with 44% (40%) *cQE* corrected quantum efficiency in

Optics EXPRESS

presence of 4 and 6 color centers in bare (coated) spherical NRs. In comparison, 8×10^5 and 2×10^6 (2×10^5 and 5×10^5) P_x *factor* can be achieved with 83% (79%) *cQE* corrected quantum efficiency in presence of 4 and 6 color centers in bare (coated) ellipsoidal NRs (Fig. 5(a), see Visualization 3(d)). Accordingly, 4×10^3 and 1×10^4 (2×10^4 and 3×10^4) $P_x cQE$ can be achieved in presence of 4 and 6 color center's in bare (coated) spherical NRs, whereas 6×10^5 and 2×10^6 (2×10^5 and 4×10^5) $P_x cQE$ can be achieved in presence of 4 and 6 color centers in bare (coated) ellipsoidal NRs. The achieved excitation and emission rate enhancements are *N*-fold larger compared to the enhancements reached via concave nanoresonators designed to enhance one single decentralized SiV center by applying similar optimization method [38], but are orders of magnitude larger than the enhancement reached via silver apertures [40,41].

The P_x *factor* and the $P_x cQE$ are always larger, when 6 color centers are embedded into a NR of the specific type. The increase of P_x and $P_x cQE$ indicates that both quantities can reach significantly larger values, when the number of emitters is increased, as it has been proven by optimizations of NRs seeded with an order of magnitude larger number of SiV color centers (not shown). However, bare spherical NRs exhibiting smaller radiative rate enhancements allow reaching smaller P_x *factor* and $P_x cQE$ in case of the same number of emitters, whereas bare ellipsoidal NRs make it possible to achieve larger P_x *factor* and $P_x cQE$ according to the larger radiative rate enhancement both at the excitation and emission wavelengths. This indicates that bare spherical NRs are less efficient, whereas bare ellipsoidal NRs are better in non-cooperative SiV fluorescence enhancement, than their coated counterparts.

The fluorescence enhancement qualified by the P_x *factor* and $P_x cQE$ is two and one orders of magnitude larger in bare and coated ellipsoidal NRs, than in their spherical counterparts, respectively (Fig. 5(a), see Visualization 3(d)). By comparing the achieved total fluorescence enhancements, one could already conclude that ellipsoidal NRs are more efficient to achieve superradiantly enhanced emission. However, from the point of view of superradiance the relative enhancements with respect to corresponding reference systems seeded with one single SiV center provide the relevant information, which are presented in the next section.

3.4. Evaluation of superradiance

Seeding with either 4 or 6 SiV color centers of all optimized NRs resulted in superradiance independently of their type and geometry. This is proven by that the balanced partial *N*-fold excitation rate enhancement threshold of superradiance is approximated or reached in spherical NRs, whereas this threshold is reached or slightly overridden in ellipsoidal NRs. Moreover, the balanced partial *N*-fold emission rate enhancement threshold is slightly and considerably overridden in spherical and ellipsoidal NRs, respectively (Fig. 5(b), see Visualization 4(a) and Visualization 5(a)). Accordingly, in all optimized plasmonically enhanced systems the threshold of superradiance is better overridden than in case of pure nanodiamonds [31].

The corrected quantum efficiency at the emission is almost the same in the optimized multiple SiV color centers seeded spherical NRs as in their reference system, only exception is bare_6 spherical NR, where *cQE* improvement is achieved (Fig. 5(b), see Visualization 4(b) and Visualization 5(b)). In contrast, all ellipsoidal NRs exhibit a significant *cQE* improvement as well. The complete multiplied N^2-fold P_x *factor* ($P_x cQE$) threshold of superradiance is overridden in bare_4 and bare_6 (in same and in coated_6) spherical NRs, it is just approximated in coated_4 and coated_6 (coated_4) spherical NRs, whereas it is overridden by both quantities in all ellipsoidal NRs (Fig. 5(b), see Visualization 4(c) and Visualization 5(c)). All ellipsoidal NRs result in larger relative enhancements, than their spherical counterparts in all quantities.

Based on the average of normalized enhancement ratios the SR threshold is slightly better overridden both in bare and coated spherical NRs consisting of 6 SiV color centers. In the presence of 6 SiV color centers, the SR threshold is more significantly overridden in bare ellipsoidal NR, whereas 4 SiV color centers result in better SR performance in coated ellipsoidal

Optics EXPRESS

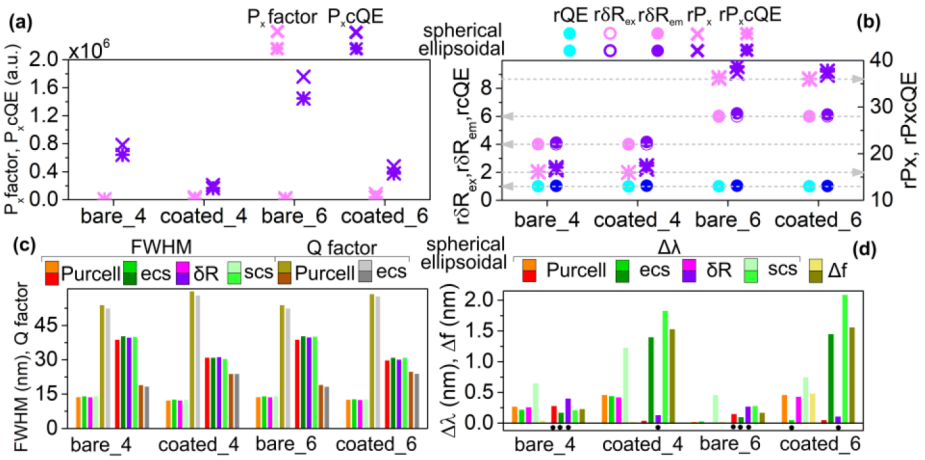

Fig. 5. (a) Comparison of the P_x *factor* and $P_x cQE$ achieved via optimized spherical and ellipsoidal NRs. (b) Comparison of δR radiative rate enhancement, cQE quantum efficiency, P_x *factor* and $P_x cQE$ to those achieved via corresponding reference systems: proof of superradiance. (c) FWHM of the *Purcell factor* and δR radiative rate enhancement peaks, extinction (*ecs*) and scattering (*scs*) cross-section peaks and the Q factor computed based on *Purcell factor* and *ecs* peaks. (d) Detuning ($\Delta\lambda$) of the *Purcell factor*, δR, *ecs* and *scs* peaks and the frequency pulling ($\Delta f = f_{ecs} - f_{\delta R}$). More details are provided in Visualization 4, Visualization 5, and Visualization 6.

NR. These results indicate that larger number of SiV color centers is advantageous in both types of spherical and in bare ellipsoidal NRs, but it turned out to be disadvantageous in coated ellipsoidal NRs (Fig. 5(b), see Visualization 5(d)). The average of normalized enhancement ratios with respect to the reference system is larger in bare spherical NRs independently of the number of emitters. In contrast, the average of normalized ratios is larger in bare ellipsoidal NR consisting of 6 SiV centers, whereas it is smaller in bare ellipsoidal NR seeded with 4 SiV color centers (see Visualization 5(d)). The better superradiance performance in case of bare composition is demonstrated in spherical NRs but only in more seeded ellipsoidal NRs.

Based on $\overline{rX}$ ellipsoidal nanoresonators ensure better superradiance performance than their spherical counterparts, independently of the embedded color center number and NR type. The presented results prove the seeding dependent effect of the nanoresonator type on superradiance performance and indicate that the quality of dielectric environment has to be considered. One has to emphasize that the controlled excitation of symmetrically arranged 4 and 6 SiV color centers can be realized similarly in bare and coated nanoresonators.

A sensitivity study on the nanoresonator shape proved that the emission rate enhancement decreases in perfect spherical, non-perfect spherical, diamond nanocrystal-shaped NR succession. Moreover, hotspots originating from non-perfect spherical NRs, and edge-effects originating from nanocrystal-shape can promote better superradiance performance. Although, the location of SiV color centers has a well-defined impact on the achieved fluorescence as well as on the overriding of SR threshold, both modify with a small rate by varying the emitter-metal distance, and the optimal configurations ensure a trade-off between them.

3.5. *Evaluation of nanoresonators*

The FWHM of the *ecs* and *scs* peaks is always larger than that of the *Purcell factor* and δR peaks in the optimized NRs, which reveals that line-width narrowing occurs in all NRs consisting of cooperatively oscillating emitters, with one single exception of coated_4 ellipsoidal NR (Fig.

Optics EXPRESS

5(c), see Visualization 6(a)). The FWHM of all inspected spectral peaks weakly depends on the number of emitters, it is uniformly larger in bare NRs than in their coated counterparts and it is larger in ellipsoidal NRs than in their spherical counterparts.

In NR evaluation one has to emphasize that to achieve a plasmonic Dicke effect operation in the bad-cavity region is preferred, therefore NRs exhibiting smaller quality factor can be proposed. The *Q factors* computed based on the *ecs* and *Purcell factor* spectra correlate, the former is slightly smaller in all inspected cases, except in coated_4 ellipsoidal NR, in accordance with the FWHM of corresponding peaks. The quality factor is smaller in case of 6 embedded color centers, when it is computed based either on *ecs* or *Purcell factor* peaks of spherical NRs, but only when it is determined based on *ecs* peaks of bare ellipsoidal NRs (Fig. 5(c), see Visualization 6(b)). The *Q factor* corresponding to *ecs* and *Purcell factor* is smaller in all bare NRs, than in their coated counterparts. The quality factor is more than two-times smaller in ellipsoidal NRs than in their spherical counterparts.

In spherical NRs detuning is smaller in case of 6 emitters, with exceptions of *Purcell factor* and δR in coated NRs. In contrast, in bare (coated) ellipsoidal NRs detuning is smaller in case of 6 emitters with the exception of *scs* (only for δR) peak. Detuning of peaks in all inspected quantities is smaller in bare spherical NRs than in their coated counterparts. In bare ellipsoidal NRs detuning of the *ecs* and *scs* peaks is smaller, whereas detuning of the *Purcell factor* and δR peaks is larger, than in coated ellipsoidal NRs. Accordingly, bare ellipsoidal NRs are capable of resulting in smaller detuning of *ecs* and *scs* peaks with respect to spherical counterparts, except the *ecs* peak in case of 6 SiV color centers. Complementarily, in coated ellipsoidal NRs detuning of *Purcell factor* and δR peaks is smaller, than in their spherical counterparts.

Small detuning of spectral peaks promotes fluorescence enhancements, however anti-correlation between detuning and the fluorescence enhancement (P_x, $P_x cQE$) and superradiance performance ($\overline{rX}$) almost uniformly exists only when one compares 6 SiV centers seeded NRs to their less seeded counterparts.

Smaller frequency pulling (Δf) accompanies smaller *Q factor* and better superradiance performance in bare spherical NR seeded with 6 color centers, whereas Δf becomes larger in coated_6 spherical NR showing the expected correlations (Fig. 5(d), see Visualization 6(d)). In comparison, Δf is smaller in bare ellipsoidal NR in accordance with the larger *Q factor*, when 6 color centers are embedded, whereas Δf becomes larger in more seeded coated ellipsoidal NR despite the larger *Q factor*. Larger Δf is reached in bare_4 spherical NRs, which correlates with the smaller *Q factor* and larger $\overline{rX}$. In bare_4 ellipsoidal NRs Δf is smaller, whereas the larger Δf correlates with the larger $\overline{rX}$ in its coated counterpart. As expected, smaller *Q factor* results in larger $\overline{rX}$ and larger Δf in all ellipsoidal NRs, than in their spherical counterparts.

3.6. Applicability in quantum information processing

Considering that symmetry breaking causes different close-neighboring environment, dephasing and frequency chirp, whereas the indistinguishable nature of emitters is an important peculiarity of Dicke effect, persistence or lifting of degeneracy has to be inspected [4]. In case of phase-synchronization 4 emitters in excitation configurations and both of 4 and 6 emitters in emission configurations are indistinguishable in all NRs due to the symmetry properties of their arrays. In contrast, two subsystems of 2 and 4 emitters located at 0° and 60° azimuthal orientation with respect to the x axis are distinguishable in excitation configuration of NRs seeded with 6 SiV color centers.

In spherical NRs the *Purcell factor* indicates a monotonous exponential decay at the excitation and a monotonous increase at the emission, when the distance of the SiV color centers is increased. Degeneracy in the *Purcell factor* at the excitation is 4-4 - (2 and 4) - (2 and 4) -fold, whereas it is at the emission is 4-4 - 6-6 -fold in bare_4 - coated_4 - bare_6 - coated_6 spherical NRs (Figs. 6(a) and 6(b), see Visualization 7).

Optics EXPRESS

In contrast, at the excitation the *Purcell factor* exhibits a non-monotonous distance dependency in all of 4 SiV color centers in bare_4 ellipsoidal NR and in a subsystem of 4 SiV color centers in bare_6 ellipsoidal NR, whereas subsystem consisting of 2 SiV color centers exhibits a monotonous increase in bare_6 ellipsoidal NR. In comparison, at the excitation the *Purcell factor* uniformly decreases exponentially in all of 4 SiV color centers in coated_4 ellipsoidal NR but differently decreases in subsystems consisting of 2 and 4 of the 6 SiV color centers in coated_6 ellipsoidal NR. In emission configuration of ellipsoidal NRs the *Purcell factor* exponentially decreases throughout small emitter distances, however a slow recovery is observable in bare ellipsoidal NRs already in the inspected distance interval. Degeneracy in the *Purcell factor* at the excitation is 4-4 - (2 and 4) - (2 and 4) -fold, whereas degeneracy at the emission is 4-4 - 6-6 -fold in bare_4 - coated_4 - bare_6 - coated_6 ellipsoidal NRs, similarly to their spherical counterparts (Figs. 6(a) and 6(b), see Visualization 7).

These results indicate that the two subsystems of emitters are distinguishable in the excitation configuration of 6 color center's seeded spherical and ellipsoidal NRs, whereas all emitters are indistinguishable in all other NR configurations. The two non-degenerated curves at the excitation converge to the same dependency at distances larger than 20 nm and 8 nm in 6 emitter's seeded spherical and ellipsoidal NRs, respectively. Based on this one has to consider that although, the threshold of superradiance is more significantly overridden in case of 6 color centers, the indistinguishable nature is preserved at both wavelengths only in case of 4 emitters arranged in a square pattern in the NRs caused by symmetry reasons.

However, the 2.6% and 14.2% splitting in bare_6 and coated_6 ellipsoidal NRs could be neglected, whereas the larger 56% splitting in 6 color centers seeded spherical NRs has to be taken into account (Figs. 6(a) and 6(b), see Visualization 7).

To select a coupled system for a specific application the trade-off between the indistinguishable nature and other properties has to be considered. Although, 4 SiV color centers are indistinguishable in both configurations of spherical and ellipsoidal NRs, in all NRs embedding 4 color centers the accompanying P_x *factor* and $P_x cQE$ are smaller. Moreover, in bare_4 spherical and ellipsoidal NRs larger detuning arises (except *scs* peak in ellipsoidal NRs), even though the frequency pulling is larger, than in their 6 color centers seeded counterparts. In coated_4 spherical NR smaller detuning is achieved only via δR, moreover Δf is smaller caused by the less perfectly met bad-cavity criterion, compared to its 6 color centers embedding counterpart. Although, in coated_4 ellipsoidal NR detuning of all spectral peaks is smaller (except that of the δR), Δf is smaller than in coated_6 ellipsoidal NR, moreover there is no line-width narrowing (Fig. 5(d), see Visualization 6).

Both the P_x factor and $P_x cQE$ are larger in systems seeded with collectively oscillating emitters than in systems seeded with the same number of randomly oscillating emitters in NRs having the parameters as those determined by optimization realized in presence of emitters with uniform collective phases (Figs. 6(c) and 6(d)). Accordingly, the optimized systems are suitable to achieve superradiantly enhanced fluorescence after synchronization. The difference between P_x *factor* and the $P_x cQE$ achievable via cooperatively oscillating and randomized systems is significantly more pronounced in ellipsoidal NRs.

Optics EXPRESS

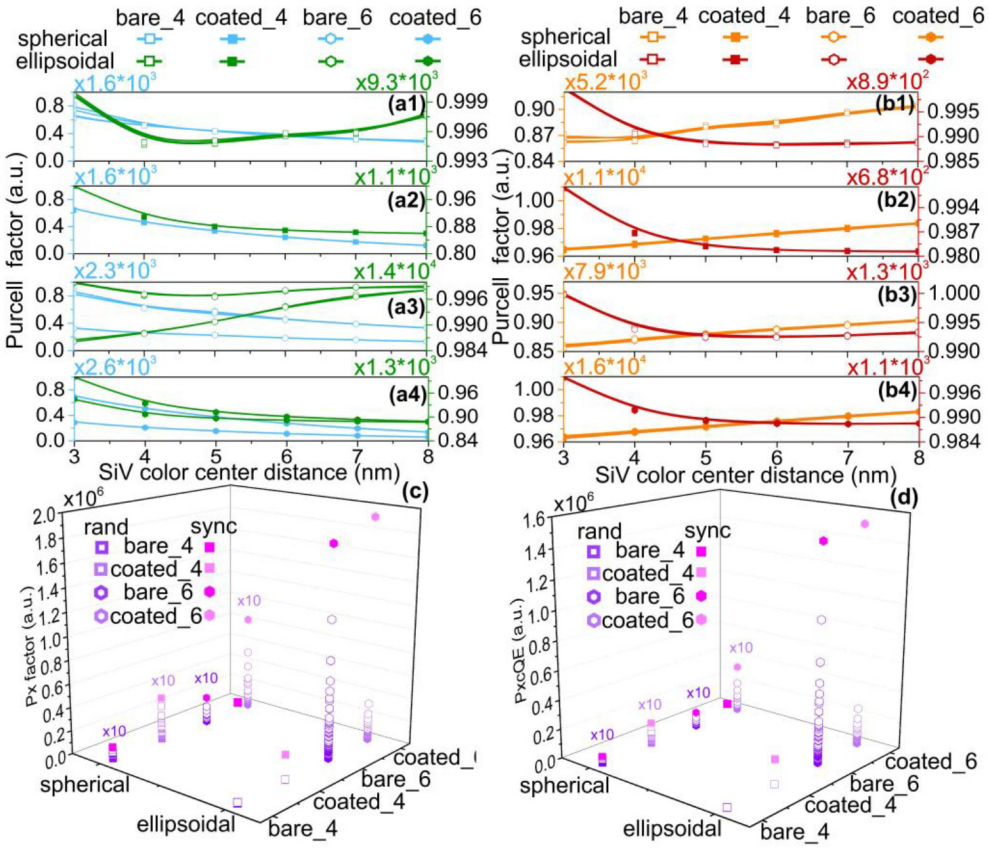

Fig. 6. Degeneracy in *Purcell factor* of the optimized (a1, b1) bare_4, (a2, b2) coated_4, (a3, b3) bare_6, (a4, b4) coated_6 NRs at the (a) excitation and (b) emission wavelengths. Comparison of the P_x *factor* and $P_x cQE$ achieved via (c) spherical and (d) ellipsoidal NRs in case of collectively and randomly oscillating emitters in the optimized NRs. More details are provided in Visualization 7.

4. Conclusions

The presented results indicate that all characteristics are less specific to the number of emitters, whereas the FWHM and the quality factor are sensitive to NR type and geometry.

The more significant overriding of superradiance threshold in both cases of 4 or 6 embedded SiV color centers shows that bare spherical NRs have advantages in cooperative fluorescence improvement. Complementarily, the significantly larger values of P_x *factor* and $P_x cQE$ indicate that coated spherical NRs are advantageous in non-cooperative fluorescence improvement. In contrast, the simultaneously larger values of P_x *factor* and $P_x cQE$ and the more significant overriding of superradiance threshold in case of 6 embedded SiV centers proves the particular advantage of more seeded bare ellipsoidal NRs in efficient superradiance generation. Complementary, in 4 SiV color center seeded coated ellipsoidal NR the relatively smaller values of P_x *factor* and $P_x cQE$ are accompanied by better superradiance performance.

Analyses of all coupled systems received via optimization revealed that the relationship between superradiance performance and quality factor depends on the number of emitters, as well as on the NR type and geometry. The interdependency of superradiance performance and *Q factor* manifest itself in coupled system type specific branches. This makes it possible that

Optics EXPRESS

better superradiance performance is achievable via coated_4 than via coated_6 ellipsoidal NR, even if its *Q factor* is just slightly smaller. Similarly, coated_4 ellipsoidal NR can exhibit better superradiance performance despite the larger *Q factor* compared to its bare counterpart.

Taking into account the complexity of the NRs characteristics, the overall ranking of the optimized coupled systems was performed by considering the achieved P_x *factor* and $P_x cQE$, the quality factor, the average of normalized ratios with respect to the reference system qualifying the extent of superradiance threshold overriding as well as the degree of detuning with respect to the SiV color center emission wavelength. This ranking resulted in the coated_4 - bare_4 - coated_6 - bare_6 spherical NR and coated_6 - coated_4 - bare_4 - bare_6 ellipsoidal NR succession. The seeding, NR type and geometry specific superradiance performance and *Q factor* relationship results in the better ranking of coated_4 ellipsoidal NR. The resulted ranking indicates that bare type NRs embedding 6 color centers, either of spherical or ellipsoidal geometry possess the most promising superradiant characteristics. Since all ellipsoidal NRs result in larger average of normalized ratios according to the smaller Q factors, than their spherical counterparts, one can conclude that the bare_6 ellipsoidal NR is the most suitable to achieve efficient superradiance. Further studies revealed that the superradiance performance improves, when the emitter's number is further increased, but saturates in case of seeding with an order of magnitude larger number of SiV color centers.

The presented results make it possible to select the right seeding, nanoresonator type and geometry, which are the most suitable to achieve non-cooperatively or superradiantly enhanced fluorescence, according to user preferences. For applications, where completely indistinguishable nature is important, we propose bare_4 ellipsoidal NR exhibiting line-width narrowing and larger frequency pulling with compromised slightly smaller fluorescence enhancement caused by larger detuning. When line-width narrowing is not required, relatively better superradiance performance can be achieved with a compromised smaller frequency pulling and smaller fluorescence caused by larger δR detuning via coated_4 ellipsoidal NR. When SiV color centers can be partially distinguishable, bare_6 type spherical and ellipsoidal NRs are better, since they exhibit better superradiance performance despite the smaller frequency pulling and larger fluorescence enhancement due to smaller detuning.

In summary, concave spherical and ellipsoidal core-shell NRs consisting of larger number of emitters and of bare type are the most suitable to reach superradiance. In contrast, coated spherical and bare ellipsoidal NRs are proposed to achieve non-cooperative fluorescence enhancement. The presented results prove that plasmonic Dicke effect accompanied by complete fluorescence rate enhancement proportional to N^2 can be achieved with a balanced radiative rate enhancement proportional to N both at the excitation and emission via optimized plasmonic NRs.

Funding

National Research, Development and Innovation Office (NKFIH) "Optimized nanoplasmonics" (K116362); European Union, co-financed by the European Social Fund "Ultrafast physical processes in atoms, molecules, nanostructures and biological systems" (EFOP-3.6.2-16-2017-00005).

Acknowledgments

Balázs Bánhelyi acknowledges that the project was supported by the János Bolyai Research Scholarship of the Hungarian Academy of Sciences. The authors acknowledge the valuable discussions with Miklós Veres about the experimental feasibility. The authors are grateful for coding of some related programs to Tamás Dániel Juhász, who was supported by the project "Integrated program for training new generation of scientists in the fields of computer science" (EFOP-3.6.3-VEKOP-16-2017-0002).

Optics EXPRESS

Disclosures

The authors declare no conflicts of interest.

References

1. R. H. Dicke, "Coherence in spontaneous radiation processes," Phys. Rev. **93**(1), 99–110 (1954).
2. B. M. Garraway, "The Dicke model in quantum optics: Dicke model revisited," Philos. Trans. R. Soc., A **369**(1939), 1137–1155 (2011).
3. R. Friedberg, S. R. Hartman, and J. T. Manassah, "Limited superradiant damping of small samples," Phys. Lett. A **40**(5), 365–366 (1972).
4. M. Gross and S. Haroche, "Superradiance: An essay on the theory of collective spontaneous emission," Phys. Rep. **93**(5), 301–396 (1982).
5. V. Degiorgio and F. Ghielmetti, "Approximate solution to the superradiance master equation," Phys. Rev. A **4**(6), 2415–2418 (1971).
6. N. E. Nefedkin, E. S. Andrianov, A. A. Zyablovsky, A. A. Pukhov, A. V. Dorofeenko, A. P. Vinogradov, and A. A. Lisyansky, "Superradiance of a subwavelength array of classical nonlinear emitters," Opt. Express **24**(4), 3464–3478 (2016).
7. N. Skribanovitz, I. P. Herman, J. C. MacGillivray, and M. S. Feld, "Observation of Dicke superradiance in optically pumped HF gas," Phys. Rev. Lett. **30**(8), 309–312 (1973).
8. J. T. Manassah, "Large swings in the forward-backward super-radiant emission direction from a nearly inverted ensemble of a three-level cascade system," Phys. Rev. A **93**(2), 023820 (2016).
9. Y. K. Wang and F. T. Hioe, "Phase transition in the Dicke model of superradiance," Phys. Rev. A **7**(3), 831–836 (1973).
10. D. Nagy, G. Szirmai, and P. Domokos, "Self-organization of a Bose-Einstein condensate in an optical cavity," Eur. Phys. J. D **48**(1), 127–137 (2008).
11. K. Baumann, C. Guerlin, F. Brennecke, and T. Esslingeret, "Dicke quantum phase transition with a superfluid gas in an optical cavity," Nature **464**(7293), 1301–1306 (2010).
12. D. Martin-Cano, L. Martin-Moreno, F. J. Garcia-Vidal, and E. Moreno, "Resonance energy transfer and superradiance mediated by plasmonic nanowaveguides," Nano Lett. **10**(8), 3129–3134 (2010).
13. V. N. Pustovit and T. V. Shahbazyan, "Cooperative emission of light by an ensemble of dipoles near a metal nanoparticle: the plasmonic Dicke effect," Phys. Rev. Lett. **102**(7), 077401 (2009).
14. V. N. Pustovit and T. V. Shahbazyan, "Plasmon-mediated superradiance near metal nanostructures," Phys. Rev. B **82**(7), 075429 (2010).
15. T. V. Shahbazyan, "Plasmonic Dicke effect," Appl. Phys. A **103**(3), 755–758 (2011).
16. V. N. Pustovit, F. Capolino, and A. Aradian, "Cooperative plasmon-mediated effects and loss compensation by gain dyes near a metal nanoparticle," J. Opt. Soc. Am. B **32**(2), 188–193 (2015).
17. I. E. Protsenko and A. V. Uskov, "Superradiance of several atoms near a metal nanosphere," Quantum Electron. **45**(6), 561–572 (2015).
18. P. Fuché, S. G. Kosionis, and P. Lalanne, "Collective scattering in hybrid nanostructures with many atomic oscillators coupled to an electromagnetic resonance," Phys. Rev. B **95**(19), 195418 (2017).
19. S. Fuchs and S. Y. Buhmann, "Purcell-Dicke effect for an atomic ensemble near a surface," https://arxiv.org/abs/1804.01265.
20. K. Sinha, B. P. Venkatesh, and P. Meystre, "Collective effects in Casimir-Polder forces," Phys. Rev. Lett. **121**(18), 183605 (2018).
21. A. A. Zabolotskii, A. Kuchyanov, F. Benimetskiy, and A. I. Plekhanov, "Collective fluorescence of composite nanoparticles," J. Exp. Theor. Phys. **126**(2), 174–182 (2018).
22. J. T. Manassah, "The Purcell-Dicke effect in the emission from a coated small sphere of resonant atoms placed inside a matrix cavity," Laser Phys. **22**(4), 738–744 (2012).
23. R. Friedberg and J. T. Manassah, "Interactive model of Purcell-Dicke enhancement," Phys. Rev. A **86**(2), 023804 (2012).
24. T. V. Teperik and A. Degiron, "Superradiant optical emitters coupled to an array of nanosize metallic antennas," Phys. Rev. Lett. **108**(14), 147401 (2012).
25. A. V. Dorofeenko, A. A. Zyablovsky, A. P. Vinogradov, E. S. Andrianov, A. A. Pukhov, and A. A. Lisyansky, "Steady state superradiance of a 2D-spaser array," Opt. Express **21**(12), 14539–14547 (2013).
26. J. G. Bohnet, Z. Chen, J. M. Weiner, D. Meiser, M. J. Holland, and J. K. Thompson, "A steady-state superradiant laser with less than one intracavity photon," Nature **484**(7392), 78–81 (2012).
27. Z. Zhang and L. M. Duan, "Quantum metrology with Dicke squeezed states," New J. Phys. **16**(10), 103037 (2014).
28. J. A. Mlynek, A. A. Abdumalikov, C. Eichler, and A. Wallraff, "Observation of Dicke superradiance for two artificial atoms in a cavity with high decay rate," Nat. Commun. **5**(1), 5186 (2014).
29. J. Ren, J. Yuan, and X. Zhang, "Multi-qubit quantum phase gates based on surface plasmons of a nanosphere," J. Opt. Soc. Am. B **31**(2), 229–236 (2014).
30. M. V. Shestakov, E. Fron, L. V. Chinotaru, and V. V. Moshchalkov, "Plasmonic Dicke effect in Ag-nanoclusters-doped oxyfluoride glasses," J. Phys. Chem. C **119**(34), 20051–20056 (2015).

Optics EXPRESS

31. C. Bradac, M. T. Johnsson, M. van Breugel, B. Q. Baragiola, R. Martin, M. L. Juan, G. K. Brennen, and T. Volz, "Room-temperature spontaneous superradiance from single diamond nanocrystals," Nat. Commun. **8**(1), 1205 (2017).
32. M. L. Juan, C. Bradac, B. Besga, M. Johnsson, G. Brennen, G. Molina-Terriza, and T. Volz, "Cooperatively enhanced dipole forces from artificial atoms in trapped nanodiamonds," Nat. Phys. **13**(3), 241–245 (2017).
33. I. I. Vlasov, A. Shiryaev, T. Rendler, S. Steinert, S.-Y. Lee, D. Antonov, M. Vörös, F. Jelezko, A. V. Fisenko, L. F. Semjonova, J. Biskupek, U. Kaiser, O. I. Lebedev, I. Sildos, P. R. Hemmer, V. I. Konov, A. Gali, and J. Wrachtrup, "Molecular-sized fluorescent nanodiamonds," Nat. Nanotechnol. **9**(1), 54–58 (2014).
34. L. J. Rogers, K. D. Jahnke, A. D. Doherty, A. Dietrich, L. P. McGuinness, C. Müller, T. Teraji, H. Sumiya, J. Isoya, N. B. Manson, and F. Jelezko, "Electronic structure of the negatively charged silicon-vacancy center in diamond," Phys. Rev. B **89**(23), 235101 (2014).
35. R. E. Evans, A. Sipahigil, D. D. Sukachev, A. S. Zibrov, and M. D. Lukin, "Narrow-linewidth homogeneous optical emitters in diamond nanostructures via silicon ion implantation," Phys. Rev. Appl. **5**(4), 044010 (2016).
36. A. Sipahigil, R. E. Evans, D. D. Sukachev, M. J. Burek, J. Borregaard, M. K. Bhaskar, C. T. Nguyenm, J. L. Pacheco, H. A. Atikian, C. Meuwly, R. M. Camacho, F. Jelezko, E. Bielejec, H. Park, M. Loncar, and M. D. Lukin, "An integrated diamond nanophotonics platform for quantum optical networks," Science **354**(6314), 847–850 (2016).
37. A. Szenes, B. Bánhelyi, L. Zs. Szabó, G. Szabó, T. Csendes, and M. Csete, "Enhancing diamond color center fluorescence via optimized plasmonic nanorod configuration," Plasmonics **12**(4), 1263–1280 (2017).
38. A. Szenes, B. Bánhelyi, L. Z. Szabó, G. Szabó, T. Csendes, and M. Csete, "Improved emission of SiV diamond color centers embedded into concave plasmonic core-shell nanoresonators," Sci. Rep. **7**(1), 13845 (2017).
39. A. Szenes, B. Bánhelyi, T. Csendes, G. Szabó, and M. Csete, "Enhancing diamond fluorescence via optimized nanorod dimer configurations," Plasmonics **13**(6), 1977–1985 (2018).
40. A. Bulu, T. Babinec, B. Hausmann, J. T. Choy, and M. Loncar, "Plasmonic resonators for enhanced diamond NV-center single photon sources," Opt. Express **19**(6), 5268–5276 (2011).
41. J. T. Choy, B. J. M. Hausmann, T. M. Babinec, I. Bulu, M. Khan, P. Maletinsky, A. Yacoby, and M. Loncar, "Enhanced single-photon emission from a diamond-silver aperture," Nat. Photonics **5**(12), 738–743 (2011).
42. S. Kumar, V. A. Davydov, V. N. Agafonov, and S. I. Bozhevolnyi, "Excitation of nanowire surface plasmons by silicon vacancy centers in nanodiamonds," Opt. Mater. Express **7**(7), 2586–2596 (2017).
43. J. Song, H. Li, F. Lin, L. Wang, H. Wu, and Y. Yang, "Plasmon-enhanced photoluminescence of Si-V centers in diamond from a nanoassembled metal–diamond hybrid structure," CrystEngComm **16**(36), 8356–8362 (2014).
44. O. Mello, Y. Li, P. Camayd-Muñoz, C. Chia, I-C. Huaang, M. Lončar, and E. Mazur, "Strongly extended superradiance in diamond metamaterials," presented at *2017 Conference on Lasers and Electro-Optics (CLEO)*, San-Jose, CA, USA, 14-19 May, 2017.
45. T. Csendes, L. Pál, J. O. H. Sendin, and J. R. Banga, "The GLOBAL optimization method revisited," Opt. Lett. **2**(4), 445–454 (2008).
46. M. Csete, D. Vass, A. Szenes, B. Bánhelyi, T. Csendes, and G. Szabó, "Plasmon enhanced fluorescence characteristics government by selecting the right objective function," presented at *Comsol Conference, Boston*, USA, 3-5 Oct. 2018.
47. I. Pócsik, M. Veres, M. Füle, M. Koós, J. Kokavecz, Z. Tóth, and G. Radnóczi, "Carbon nano-particles prepared by ion-clustering in plasma," Vacuum **71**(1–2), 171–176 (2003).
48. P. B. Johnson and R. W. Christy, "Optical constants of the noble metals," Phys. Rev. B **6**(12), 4370–4379 (1972).
49. P. E. Barclay, K.-M. C. Fu, C. Santori, A. Faraon, and R. G. Beausoleil, "Hybrid nanocavity resonant enhancement of color center emission in diamond," Phys. Rev. X **1**(1), 011007 (2011).
50. O. Lehtinen, B. Naydenov, P. Börner, K. Melentjevic, C. Müller, L. P. McGuinness, S. Pezzagna, J. Meijer, U. Kaiser, and F. Jelezko, "Molecular dynamics simulations of shallow nitrogen and silicon implantation into diamond," Phys. Rev. B **93**(3), 035202 (2016).